Numerical Investigation on a Dual-jet Consisting of a Plane Wall Jet and a Parallel Offset Jet at Low-Reynolds Number

Zhao Liqing[1*], *Sun Jianhong*[2]

1. School of Marine Sciences, Nanjing University of Information Science & Technology, Nanjing 210044, P. R. China;
2. College of Aerospace Engineering, Nanjing University of Aeronautics and Astronautics, Nanjing 210016, P. R. China

(Received 30 October 2017; revised 12 March 2018; accepted 18 March 2018)

Abstract: A dual-jet consisting of a wall jet and an offset jet has been numerically simulated using lattice Boltzmann method to examine the effects of jet spacing between two jet centerlines, defined as s. The Reynolds number based on jet-exit-width d is set to be $Re = 56$ and the jet spacing is set to be less than or equal 10 times the jet-exit-width. Computational results reveal that the flow field displays periodic vortex shedding when the jet spacing is in the range of $9 \leqslant s/d \leqslant 10$, while it remains steady with two counter-rotating vortices in the converging region when $s/d \leqslant 8$. When $s/d = 9$, the power spectral analyses indicate that the vortex shedding phenomenon has specific frequency. The significant oscillation stresses induced by the periodic components of velocities are found to mainly exist in the inner shear layer regions, implying stronger momentum transfer occuring in these regions.

Key words: dual-jet; low-Reynolds number; lattice Boltzmann method; vortex shedding

CLC number: O358 **Document code**: A **Article ID**: 1005-1120(2018)05-0778-11

0 Introduction

Jets are important in a variety of engineering applications, such as entrainment and mixing processes in microcircuit cooling system, ventilation system, waste disposal, and fuel injection systems[1-4]. Besides free parallel jets, the combinated wall and offset jets are also frequently encountered in many industrial processes especially in the wastewater evacuation process which makes interesting to study the dynamic characteristics of this type of flow. The combinated wall and offset jets flow consist of a lower wall jet and a upper offset jet. The lower wall jet is generated when a flow is injected into a region near the wall with an initial momentum. The upper offset jet refers to a flow issuing above a wall which is parallel to the axis of the jet. When the height of the offset is zero, the offset jet will become a wall jet.

A schematic diagram of the combinated wall and offset jets, as modified from previous studies on free parallel plane jets[5], is shown in Fig. 1. The origin of the coordinate system is set at the intersection of the jet exit plane and the bottom wall, where x is along the wall. The two jets, having the same width d, are separated in the vertical (y) direction by a distance, s. As shown in Fig. 1, there exist three distinct regions, a converging region, a merging region and a combined region. A sub-atmospheric pressure zone close to the nozzle plate causes the individual jets to curve towards each other in a region known as the converging region. The two jets merge together at some downstream position (x_{mp}, y_{mp}), known as the merging point which is characterised by the point where velocity is zero. Downstream from the merging point in the merging region, the two jets continue to interact with each other up to the combined point (x_{cp}, y_{cp}), where the deflection point originally in the mid-part of streamwise velocity profile disappears. Downstream from the

* Corresponding author, E-mail address: zhaoliqing@nuist.edu.cn.

How to cite this article: Zhao Liqing, Sun Jianhong. Numerical investigation on a dual-jet consisting of a plane wall jet and a parallel offset jet at low-Reynolds number[J]. Trans. Nanjing Univ. Aero. Astro., 2018,35(5):778-788.
http://dx.doi.org/10.16356/j.1005-1120.2018.05.778

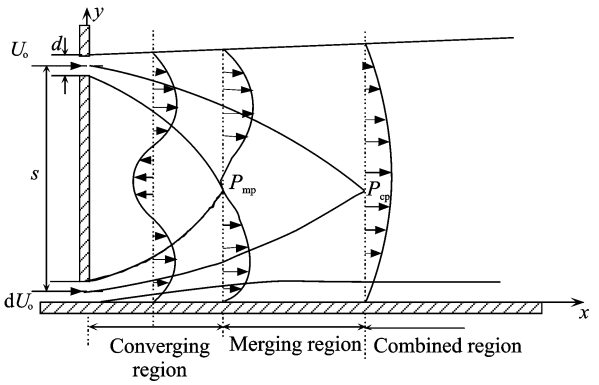

Fig. 1 Schematic of combinated wall and offset jet(s is the spacing between two jet centerlines, d the jet-exit-width, and U_o the jet-exit-velocity)

point in the combined region, the two jets combine to behave like a single wall jet.

combined Wang et al.[6] have experimentally studied the flow characteristics of the combinated wall and offset jets for a Reynolds number Re = 10 000 and an offset ratio s/d = 2. Results revealed that the near filed of the dual-jet flow is characterized by periodic Karman-like vortex street in the inner shear layer regions. The existence of the vortex shedding phenomenon results in periodic interaction between the wall jet and the offset jet. Kumar et al.[7] have numerically studied the flow characteristics of the combinated wall and offset jets for a ralatively larger value of offset ratio s/d = 9 when Re = 20 000. Their results focused on the mean flow and turbulence characteristics of the combinated dual-jet. However, no vortex shedding phenomenon was reported in this paper. Later on, Li et al.[8] numerically investigated the interaction between the plane wall jet and the parallel offset jet besed on large eddy simulation (LES). The considered Reynolds number and the offset ratio were the same as that of Wang and Tan[6]. By means of statistical analysis, they have characterized the interaction between the two jets. The results also included mixing characteristics of the two jets and were in good agreement with the experimental results of Wang and Tan[6], but did not contain any information relating to the vortex shedding phenomenon. In another paper, Li et al.[9] studied the interaction between a wall jet and an offset jet with different velocity and offset ratio using several turbulence models. Similarily, they presented only the steady state results and no vortex shedding phenomenon was reported.

In the study of Mondal et al.[10], the effect of offset ratio on the flow states was investigated when Re = 10 000 and $1.5 \leqslant s/d \leqslant 3.5$. Results showed that when s/d lies in the range $1.7 \leqslant s/d \leqslant 3.1$, the near field of the flow domain is characterized by a periodic large scale vortex shedding phenomenon. Howerer, outside this range, two steady counter rotating vortices appear in this flow zone. Mondal et al.[11] numerically investigated the effect of velocity ratio (U_r) between the inlet velocity of the wall jet (U_w) and the inlet velcity of the offset jet (U_o) on the unsteady flow structure of this type of flow. Results showed that when the velocity ratio lies in the range $0.78 \leqslant U_r \leqslant 1.34$, a periodic vortex shedding phenomenon occurs close to the nozzle plate. On the contrary, this periodic phenomenon ceases if $U_r \leqslant 0.77$ and $U_r \geqslant 1.35$. When the velocity ratio is set to 0.77 and 1.35, two stable counter rotating vortices appear in the wall vicinity along the converging zone. Recently, Mondal et al.[12] numerically investigated the effect of the bottom wall proximity on the unsteady flow state of the two jets. Here, the unsteady periodic vortex shedding phenomenon and steady state with two counter-rotating vortices were respectively observed in the flow filed.

According to the literature survey on the area of combinated wall jet and offset jet flow, only few studies[6, 10-12] report vortex shedding phenomenton. It has been reported that periodic oscillation of dual-jet can cause enhanced mixing between the jets with the ambient and has the advantages of both passive and active mixing control[1]. The literature above mainly focused on high-Reynolds number parallel plane jets, i. e. $Re > 10^3$. However, in microelectronic cooling systems, the air velocities are small, hence, low-Reynolds number jets are more relevant. However, low-Reynolds numbers combinated wall jet and offset jet flow (i. e. $Re < 10^2$) has not been

well documented in the literature. The present study is an attempt to investigate the flow characteristics of this type of flow at low-Reynolds number. The periodic vortex shedding phenomenon is also examined based on the instantaneous flow field. More in-depth study on low-Reynolds number combinated dual jet is also useful to provide improved fundamental understanding of the jet stability and transition to turbulence. In most numerical solvers, the flow field is obtained by solving the Navier-Stokes equations. As an alternative computational technique to Navier-Stokes equations, the lattice Boltzmann method (LBM)[13] is employed to investigate the dual jets. The simulation methodology is described in Section 1. The mean flow characteristics of the dual jets are examined. The instantaneous vortex structures are visualized, which displays the existence of periodic vortex shedding, followed by a quantitative analysis of oscillation frequency.

1 Simulation Methodology

As shown in Fig. 2, the lower wall jet and upper offset jet enter into the computational domain of $60d \times 160d$ from two jet nozzles, where d is the jet-exit-width. In order to isolate the interior of the domain from the effects of the outlet boundary condition, a buffer zone is employed near the downstream end of the computational domain. The origin of the coordinate system is set at the intersection of the jet exit plane and the bottom wall, where x is along the wall. The two jets having the same width d, are separated in the vertical (y) direction by a distance s. The combinated wall jet and offset jet flow, assumed as a two-dimensional, incompressible flow, is influenced by two dimensionless parameters. One is the Reynolds number, defined as $Re = \dfrac{U_{oc} d}{\nu}$, where U_{oc} is the maximum jet-exit-velocity and ν the kinematic viscosity. Another parameter is the jet spacing s/d, where s is the spacing between two jet centerlines. In the present study, the Reynolds number is set to be $Re = 56$ and the jet spacing is set to be $s/d \leqslant 10$.

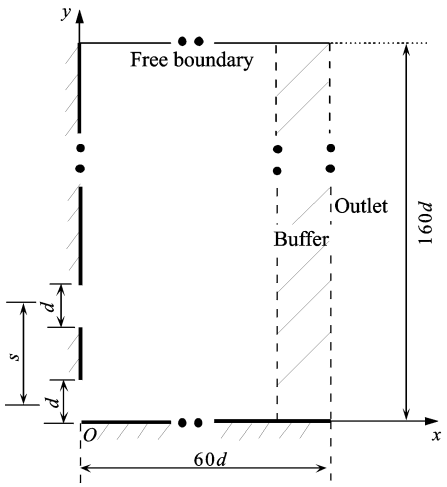

Fig. 2 Sketch of computational domain

1.1 Governing equations and boundary conditions

The governing equations of the jet flow are incompressible Navier-Stokes (N-S) equations, shown as

$$\frac{\partial u_i}{\partial x_i} = 0 \tag{1}$$

$$\frac{\partial u_i}{\partial t} + u_j \frac{\partial u_i}{\partial x_j} = -\frac{1}{\rho}\frac{\partial p}{\partial x_i} + \frac{\partial}{\partial x_j}\left(\nu \frac{\partial u_i}{\partial x_j}\right) \tag{2}$$

where u_i is the velocity, p the pressure field, ν the kinematic viscosity, and x_i the spatial coordinate. The subscripts i and j represent the spatial directions.

At each jet exit, a fully developed parabolic velocity profile is prescribed as

$$u(y) = U_{oc}\left[1 - \left(\frac{2y}{d}\right)^2\right], v = 0 \tag{3}$$

On the free boundaries, as shown in Fig. 2, the pressure is prescribed as the ambient pressure p_∞ and the other variables are extrapolated from the interior solution, allowing for entrainment. A convective boundary condition[14] is adopted at outlet boundary, shown as

$$\frac{\partial \hat{u}_i}{\partial t} + U_{con} \frac{\partial \hat{u}_i}{\partial n} = 0 \tag{4}$$

where $\hat{u}_i$ is the target velocity at outlet boundary, and U_{con} a pre-selected convection velocity in the normal direction (n) respect to the boundary. The pre-selected convection velocity is chosen to be 0.5 in the streamwise boundary[15] in the present study. In addition, a buffer zone[15-17] is employed near the downstream end of the computational domain with a length of $20d$, as shown in

Fig. 2, in order to isolate the interior of the domain from the effects of the boundary condition. Inside the buffer zone, a fringe function term[15] is added into the right-hand-side of Eq. (2), and then we have

$$\frac{\partial u_i}{\partial t}+u_j\frac{\partial u_i}{\partial x_j}=-\frac{1}{\rho}\frac{\partial p}{\partial x_i}+\frac{\partial}{\partial x_j}\left(v\frac{\partial u_i}{\partial x_j}\right)-\sigma(n)(u_i-\hat{u}_i) \tag{5}$$

where u_i is local velocity of fluid and $\hat{u}_i$ the velocity at outlet boundary obtained from the convection boundary condition Eq. (4). $\sigma(n)$ is the damping term, and its function has an exponential form[15] with streamwise position dependent part that contains the start and end position of the damping zone x_s and x_e, that is

$$\sigma(n)=\alpha\left(\frac{x-x_s}{x_e-x_s}\right)^{\beta} \tag{6}$$

where constants α and β are used to control the maximum damping parameter and the exponential growth rate, respectively. For the present study, $\alpha=0.001$ and $\beta=3$ are used.

1.2 Lattice Boltzmann method

The lattice Boltzmann method (LBM) is employed to solve the N-S Eqs. (1) and (5) in the present work. The fringe functions in Eq. (5) is dealt as an artificial body force[18] acting on the traditional N-S Equation. The lattice Boltzmann equation with the single-relaxation-time BGK approximation and the force term can be written as

$$f_\alpha(x+e_\alpha\Delta t,t+\Delta t)-f_\alpha(x,t)=-\frac{1}{\tau}[f_\alpha(x,t)-f_\alpha^{eq}(x,t)]+\Delta tF_\alpha \tag{7}$$

where $f_\alpha(x,t)$ is the distribution function for particles with velocity e_α at position x and time t, f_α^{eq} the local equilibrium distribution function of particles, Δt the time step, τ the dimensionless single-relaxation-time, which controls the rate of approach to equilibrium, and e_α the velocity vector of a particle in the link α, which can be defined in the D2Q9 model[19] as

$$e_\alpha=\begin{cases}[0,0] & \alpha=0\\ [\cos((\alpha-1)\pi/2),\sin((\alpha-1)\pi/2)] & \alpha=1,2,3,4\\ [\cos((2\alpha-9)\pi/4),\sin((2\alpha-9)\pi/4)] & \alpha=5,6,7,8\end{cases} \tag{8}$$

The force term F_α in Eq. (7) is[18]

$$F_\alpha=w_\alpha\frac{e_\alpha\cdot F}{c_s^2} \tag{9}$$

where $F=(F_x,F_y)$, $w_0=4/9$, $w_\alpha=1/9$ for $\alpha=1$—4, and $w_\alpha=1/36$ for $\alpha=5$—8 are weighting factors; $c_s=1/\sqrt{3}$ is the sound speed of the model; f_α^{eq} is the equilibrium distribution function

$$f_\alpha^{eq}=w_\alpha\rho\left[1+\frac{e_\alpha\cdot u}{c_s^2}+\frac{(e_\alpha\cdot u)^2}{2c_s^4}-\frac{|u|^2}{2c_s^2}\right] \tag{10}$$

where ρ and $u=(u,v)$ are the fluid density and velocity vector, respectively, which can be obtained by the distribution function

$$\rho=\sum_\alpha f_\alpha \tag{11}$$

$$\rho u=\sum_\alpha e_\alpha f_\alpha \tag{12}$$

Through the Chapman-Enskog procedure, the macroscopic N-S Eqs. (1), (5) can be derived from the above lattice Boltzmann BGK model in Eq. (7) and the kinematic viscosity is related to the relaxation time τ

$$\nu=\left(\tau-\frac{1}{2}\right)c_s^2\Delta t \tag{13}$$

1.3 Validation

There was little experimental study on combinated wall jet and offset jet flow at low-Reynolds numbers (i. e. $Re<10^2$) in the literature. However, there are a few experimental studies on single plane jet at low-Reynolds numbers[20, 21]. Therefore, the measurements of single plane jet at $Re=42$ by Sato et al.[20] are used as a reference to verify the present computational procedure. Fig. 3 shows the mean streamwise velocity $\langle u\rangle$ distribution of a single plane jet when $Re=42$. As expected, the velocity on the centerline of the jet decreases and the width of the jet increases downstream. It is observed that the numerical results are in agreement with the experimental data[20], which also validates the reliability of the present work.

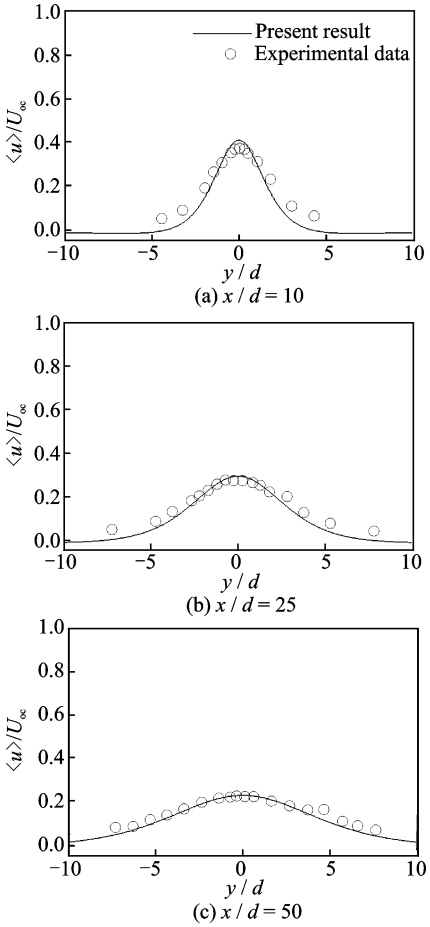

Fig. 3 Mean streamwise velocity comparing with the experimental data[20] of a single plane jet when $Re = 42$

2 Results and Discussion

2.1 Mean flow characteristics

The combinated wall and offset jets are kept at a spacing range $s/d \leqslant 10$ for this study and the Reynolds number considered here is 56. The mean velocity distribution illustrates the spatial development of the flow field. Fig. 4 shows the mean velocity magnitude contours and streamlines for different offset ratio $s/d = 6$, 8, 9 and 10. The velocity is normalized with respect to the maximum jet-exit-velocity U_{oc}. As seen from Fig. 4, each converging region is characterized by a recirculation flow, inside which two counter-rotating vortices are genenrated. The upper offset jet and lower wall jet merge together at merging point (mp), which is characterised by the point where velocity is zero. Downstream from the merging point, the two jets continue to interact with each other up to the combined point (cp). Downstream from the combined point, the two jets combine to behave like a single wall jet.

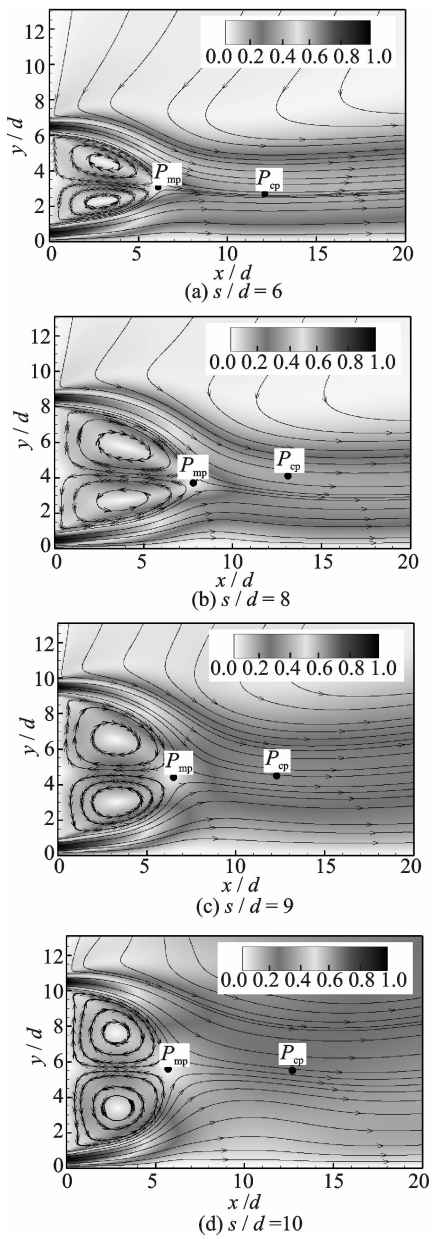

Fig. 4 Streamlines and mean velocity magnitude contours for different offset ratio

To see clearly the velocity profile along streamwise section, Fig. 5 shows the mean streamwise velocity profile for $s/d = 9$. The velocity is normalized with respect to the maximum jet-exit-velocity U_{oc}, while the y coordinate is normalized with jet-exit-width d. As seen in Fig. 5(a), in the converging region ($x/d < 6.5$), the maximum velocity of the offset jet decreases and the jet width increases with the increase in the stream-

wise distance from the offset plate. In the region surrounded by two jets, there is a recirculation zone where the velocity is negative. The negative velocity becomes positive after the merge point ($6.5d$, $4.4d$). Downstream from the merging point, the two jets continue to interact with each other up to the combined point ($12.3d$, $4.5d$), where the deflection point originally in the mid-part of streamwise velocity profile disappears. Downstream from the combined point, the two jets combine to behave like a single wall jet, as shown in Fig. 5(b).

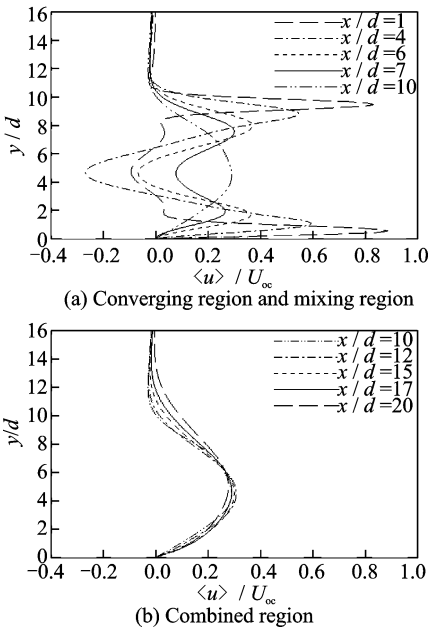

Fig. 5 Mean streamwise velocity distributions for $s/d = 9$

2.2 Instantaneous vortex structures

After issuing from the nozzles, the upper offset jet and lower wall jet merge together in the converging region forms a recirculation zone between them, as indicated in Fig. 1. The present study reveals that the flow features of the recirculation zone depend on the jet spacing between two jets, which is s/d. With the help of instantaneous vorticity contours, the dynamic interaction between the two jets in the recirculation zone are described for various values of s/d, as shown in Figs. 6(a)—(d). For the present two-dimensional study, the vorticity is computaed using the expression $w = \left(\frac{\partial v}{\partial x} - \frac{\partial u}{\partial y}\right)$. The solid lines in Fig. 6 indicate

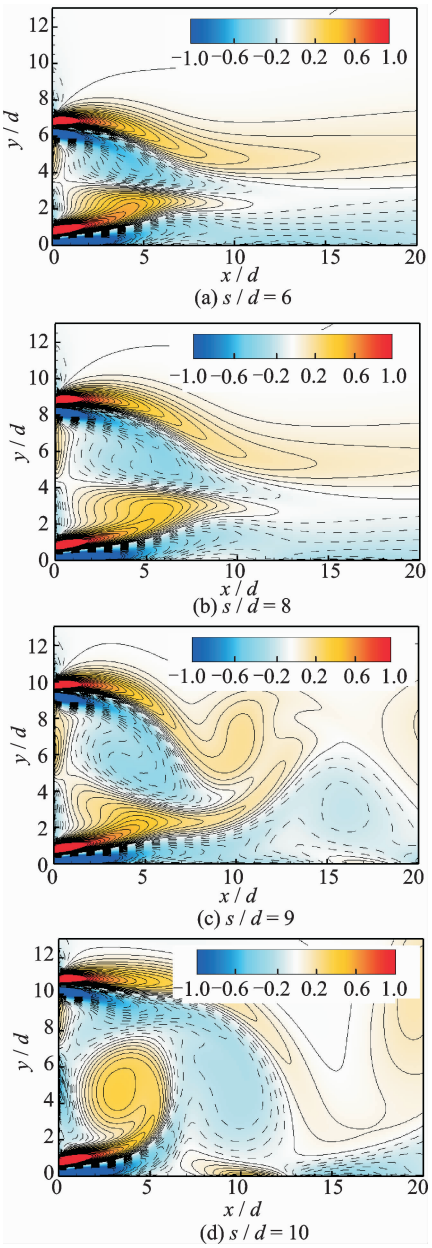

Fig. 6 Instantaneous vorticity contours of the combinated offset and wall jet for different jet spacing s/d at $t = 3\,000d/U_{oc}$

positive vorticity, whereas the dashed lines indicate negative vorticity. There exist a wall boundary layer and an inner shear layer for the lower wall jet, as well as an outer free shear layer and an inner shear layer for the upper offset jet. When $s/d = 6$ and 8, as shown in Figs. 6(a), (b), a pair of stable vortices are formed one above the other and all the four layers develop independently without any interaction between the adjacent layers. When the value of s/d is slightly increased to 9, on the contrary, discrete vortices

are induced by the interaction between inner shear layers and will shed downstream generating a well-organized vortical structure (Figs. 6(c), (d)). As a result, an unsteady time-periodic flow phenomenon occurs close to the nozzle plate similar to the flow behavior in the near wake region for flow over a vertical flat plate[22].

To demonstrate the unsteady interation process between shear layers, Fig. 7 illustrates the instantaneous vorticity contours during a time period T at an interval of $T/4$. Note that the starting time in Fig. 7 is arbitrary. As depicted, the discrete vortices are formed in the converging region of two jets. Within time period T, an upper row of negative vortices (noted as A) and a lower row of positive vortices (noted as B) are alternately grow, shed and convected downstream forming a well-organized vortex street. From Fig. 7(a) to Fig. 7(c), the upper negative vortex A is seen to grow in size and strength before it becomes strong enough to cut off the lower positive vortex B to shed downstream at $T/2$. Similarly, from Fig. 7(c) to Fig. 7(e), the lower positive vortex B is seen to grow in size and strength before it becomes strong enough to cut off the upper negative vortex A to shed at T. In the successive time periods, this phenomenon repeats itself generating the alternate shedding of vortices.

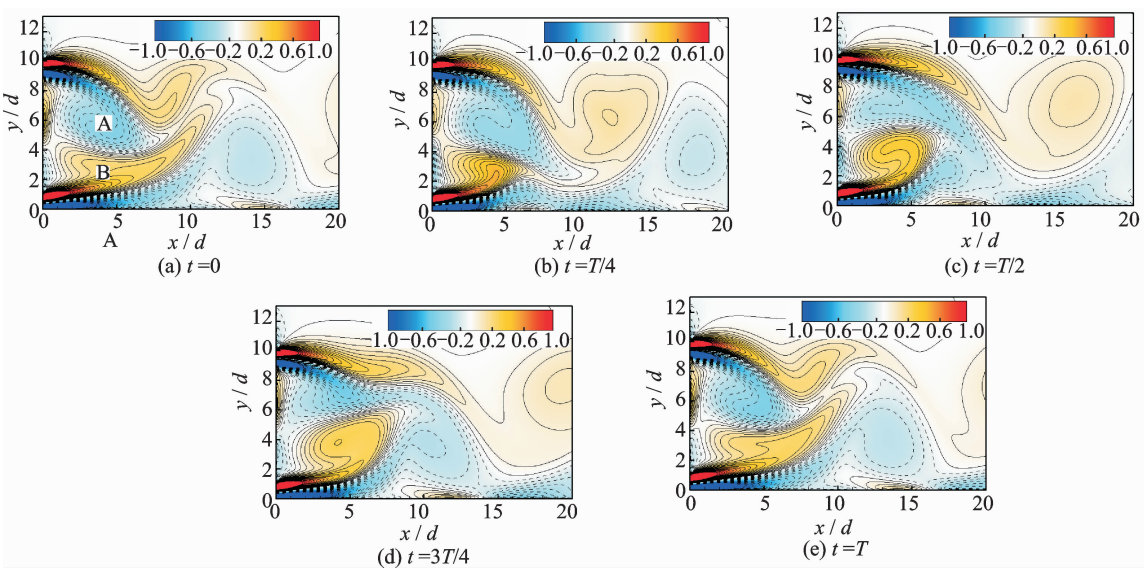

Fig. 7 Instantaneous vorticity contours for $s/d = 9$ at different instants within one time period

2.3 Instantaneous velocity and oscillation frequency

From the above anaylyses, it can be seen that there exist two flow patterns for the combinated wall and offset jets. When the jet spacing is in the range of $9 \leqslant s/d \leqslant 10$, the flow field displays periodic vortex shedding, while it remains steady with two counter-rotating vortices in the converging region when $s/d \leqslant 8$. To capture the unsteady variation of the two flow patterns, the time histories of streamwise (u) and transverse (v) velocities are recorded at two stationary points. For the present study, the stationary points are chosen at Point A ($2d$, $2d$) in the converging region and Point B ($15d$, $2d$) in the combined region. Figs. 8(a), (b) shows the time series of u and v velocity components at Point A and B for $s/d = 8$. It can be seen that both velocities remain constant, indicating a steady state behavior. For $s/d = 9$, Figs. 9(a), (b) shows the time series of u and v velocities at Points A and B, respectively. It can be seen that all velocities exhibit periodic oscillations due to the interaction between inner shear layers. To obtain the frequency of the oscillation, the power spectral densities (PSDs) of velcoities at Points A and B are shown

in Figs. 10(a),(b). The non-dimensional characteristic frequency is defined as $St = fd/U_{oc}$, where f is the dimensional oscillation frequency. For Point A and Point B, as shown in Figs. 10 (a),(b), both u-velocity and v-velocity have the same characteristic frequency, $St_{u,v} = 0.012$, indicating the frequency of vortex shedding.

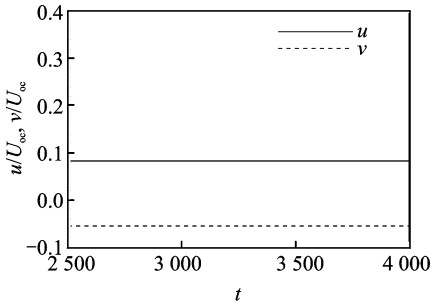

(a) Time series of u and v velocities at Point A

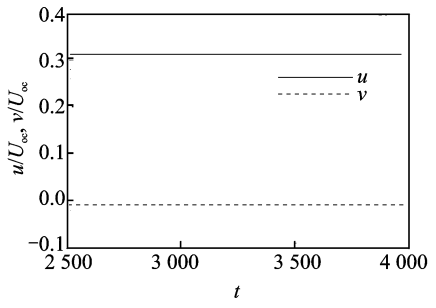

(b) Time series of u and v velocities at Point B

Fig. 8 Time series of u and v when $s/d = 8$

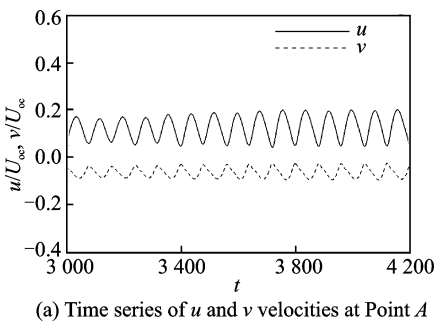

(a) Time series of u and v velocities at Point A

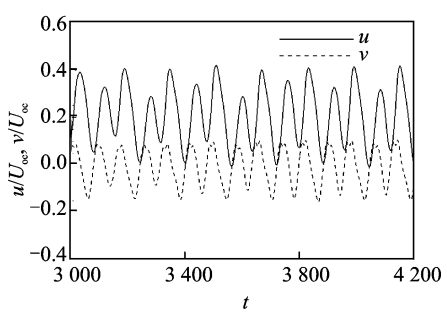

(b) Time series of u and v velocities at Point B

Fig. 9 Time series of u and v when $s/d = 9$

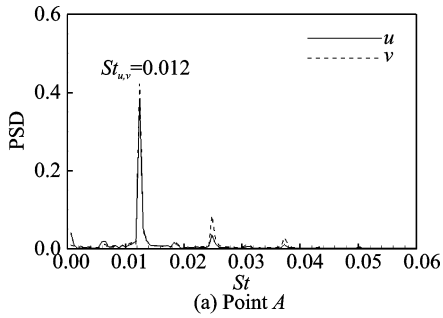

(a) Point A

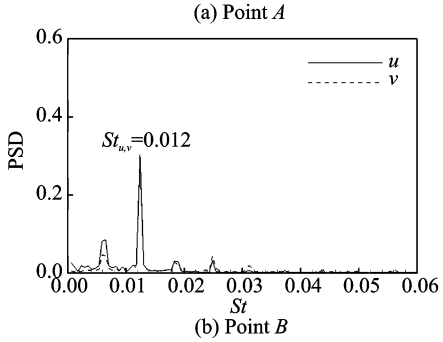

(b) Point B

Fig. 10 PSDs of velocities exhibited in Fig. 9

From the above analyses on velocity components, we can see that there exists periodic oscillation phenomenon in the flow field. If the velocities exhibit periodic components, it could be decomposed as

$$u = \langle u \rangle + \tilde{u} \tag{14}$$

$$v = \langle v \rangle + \tilde{v} \tag{15}$$

where "$\langle\rangle$" denotes the time-averaged component and "$\sim$" the periodic component. Compared to the time-averaged components, the amplitude of the periodic components could be evaluated by the root-mean-square values, $(\tilde{u})_{rms}$ and $(\tilde{v})_{rms}$, which are also the standard deviations of u and v. The magnitudes of $(\tilde{u})_{rms}$ and $(\tilde{v})_{rms}$ represent the degree of oscillation of fluid particles. The interaction between $\tilde{u}$ and $\tilde{v}$ can be evaluated by $\frac{\langle \tilde{u}\tilde{v} \rangle}{U_{oc}^2}$, which is also the covariance of velocities of u and v. The contour plots of the normalized oscillation stresses, i. e., $\frac{(\tilde{u})_{rms}}{U_{oc}^2}$, $\frac{(\tilde{v})_{rms}}{U_{oc}^2}$ and $\frac{\langle \tilde{u}\tilde{v} \rangle}{U_{oc}^2}$, are shown in Figs. 11(a)—(c), respectively for $s/d = 9$. It can be seen that all the three stresses are asymmetric about $y/d = 5$, and the intensity and growth of the several shear layers are different in the jet near field. As shown in Fig. 11(a), the

maximum of $\frac{(\tilde{u})_{\mathrm{rms}}}{U_{\mathrm{oc}}^2}$ are about 0.027 and 0.024, respectively, for the upper inner shear layer and lower inner shear layer. It is also shown that near the wall region, there are two local maxima values of $\frac{(\tilde{u})_{\mathrm{rms}}}{U_{\mathrm{oc}}^2}$, occurring at $(x/d,\ y/d) = (7.4,\ 1.5)$ and $(12,\ 1.6)$, respectively. However, no significant values of $\frac{(\tilde{v})_{\mathrm{rms}}}{U_{\mathrm{oc}}^2}$ and $\frac{\langle\tilde{u}\tilde{v}\rangle}{U_{\mathrm{oc}}^2}$ are found in the near-wall region. The maximum of $\frac{(\tilde{v})_{\mathrm{rms}}}{U_{\mathrm{oc}}^2}$ in Fig. 11(b) is 0.054 occurring at $(x/d,\ y/d) = (7.0,\ 4.7)$. In Fig. 11(c), the solid lines indicate positive values, whereas the dashed lines indicate negative values. It is shown that the significant shear stresses in Fig. 11(c) occur over the range $1.6 \leqslant x/d \leqslant 9$. In the outer layer region, the values of $\frac{(\tilde{u})_{\mathrm{rms}}}{U_{\mathrm{oc}}^2}$, $\frac{(\tilde{v})_{\mathrm{rms}}}{U_{\mathrm{oc}}^2}$ and $\frac{\langle\tilde{u}\tilde{v}\rangle}{U_{\mathrm{oc}}^2}$ are all small. All these above indicate that significant stresses always exist in the two inner shear layer regions $(1 \leqslant y/d \leqslant 9)$, which would enhance momentum transfer in these regions.

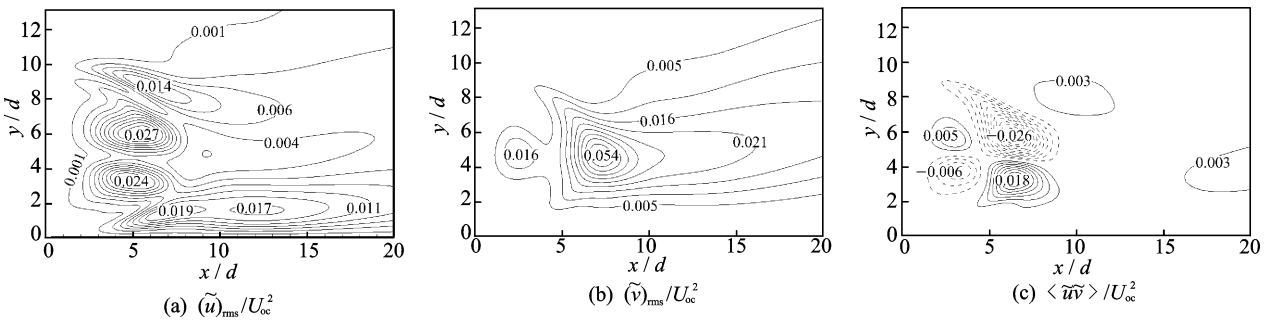

(a) $(\tilde{u})_{\mathrm{rms}}/U_{\mathrm{oc}}^2$ (b) $(\tilde{v})_{\mathrm{rms}}/U_{\mathrm{oc}}^2$ (c) $\langle\tilde{u}\tilde{v}\rangle/U_{\mathrm{oc}}^2$

Fig. 11 Contour plots of the oscillation stresses

To quantify the effect of the periodic oscillation on the flow field, Table 1 presents the location of merging point and combined point. When $s/d \leqslant 8$, the streamwise distance of merging point and combined point from the nozzle plate are found to increase with increasing s/d, which is also noted by others[10, 23]. However, when $s/d=9$, there exists an apparently decrease for the streamwise distance of both the merging point and combined point, which indicates the merging process starts at a shorter downstream distance for $s/d = 9$ than that in the case of $s/d = 8$. Meanwhile, the combinated jets for $s/d = 9$ requires shorter distance than that of $s/d = 8$ for complete merging to occur. This is attributed to the existence of periodic oscillation, where strong momentum transfer occurs in the converging region when $s/d = 9$. For the flow field, as the increase of s/d, there exist two distinguishing flow states. When $9 \leqslant s/d \leqslant 10$, the flow field displays periodic vortex shedding, while it remains steady with two counter-rotating vortices in the converging region when $s/d \leqslant 8$. The transition from steady state to periodic oscillation state as s/d is varied is worthy examination both in studying the approach to turbulence and in its own right.

Table 1 Location of merging point and combined point for different offset ratio

Parameter	$s/d=4$	$s/d=6$	$s/d=8$	$s/d=9$	$s/d=10$
$(x_{\mathrm{mp}}/d,\ y_{\mathrm{mp}}/d)$	(3.9, 2.4)	(6.1, 3.1)	(7.8,3.7)	(6.5, 4.4)	(5.7, 5.6)
$(x_{\mathrm{cp}}/d,\ y_{\mathrm{cp}}/d)$	(9, 1.9)	(12.1, 2.7)	(13.1, 4.1)	(12.3, 4.5)	(12.7, 5.5)

3 Conclusions

The flow features of low-Reynolds number dual jet consisting of a plane wall jet and a parallel offset jet are investigated for $s/d \leqslant 10$ using lattice Boltzmann method. The Reynolds number based on jet-exit-width d is set to be 56. The mean flow in the converging region is characterized by a recirculation flow, inside which two counter-rotating vortices are genenrated. The mean features in the combined region resemble a single wall jet. The instantaneous vorticity contours indicate that when $9 \leqslant s/d \leqslant 10$, the flow field displays periodic vortex shedding, while it remains steady with two counter-rotating vortices in the converging region when $s/d \leqslant 8$. When $s/d = 9$, the non-dimensional periodic oscillation frequency (Strouhal number) is found to be 0.012, indicating the frequency of vortex shedding. For $s/d \leqslant 8$, the streamwise distances of the merging point and the combined point from the nozzle plate are found to increase with increasing s/d. When $s/d = 9$, there exists an apparent decrease for both the merging point and the combined point, which indicates that the merging process starts at a shorter downstream distance for $s/d = 9$ than that in the case of $s/d = 8$. Meanwhile, the twin jets for $s/d = 9$ require shorter distance than that in the case of $s/d = 8$ for complete merging to occur.

Acknowledgements

This work was supported by the National Natural Science Foundation of China (No. 11402124), the Natural Science Foundation of Jiangsu Province (No. BK20140985), the Natural Science Foundation of Jiangsu Higher Education Institutions of China (No. 14KJB130002), and the Startup Foundation for Introducing Talent of NUIST (No. 2013x031).

References:

[1] BUNDERSON N E, SMITH B L. Passive mixing control of plane parallel jets [J]. Experiments in Fluids, 2005, 39(1): 66-74.

[2] DURVE A, PATWARDHAN A W, BANARJEE I, et al. Numerical investigation of mixing in parallel jets [J]. Nuclear Engineering and Design, 2012, 242: 78-90.

[3] GHAHREMANIAN S, SVENSSON K, TUMMERS M J, et al. Near-field mixing of jets issuing from a array of round nozzles [J]. International Journal of Heat and Fluid Flow, 2014, 47: 84-100.

[4] ZHOU T, SUN J H, LIU K. Experimental analysis and application of oxygen transfer performance of micro-bubble jet aerator [J]. Journal of Nanjing University of Aeronautics & Astronautics, 2014, 46(6): 915-919. (in Chinese)

[5] ZHAO L Q, WANG X C. Numerical investigation of parallel plane jets at low-Reynolds number [J]. European Journal of Mechanics / B Fluids, 2018, 67: 211-219.

[6] WANG X, TAN S. Experimental investigation of the interaction between a plane wall jet and a parallel offset jet [J]. Experiments in Fluids, 2007, 42(4): 551-562.

[7] KUMAR A, DAS M K. Study of a turbulent dual jet consisting of a wall jet and an offset jet [J]. Journal of Fluids Engineering, 2011, 133(10): 1201-1211.

[8] LI Z W, HUAI W X, HAN J. Large eddy simulation of the interaction between wall jet and offset jet [J]. Journal of Hydrodynamics, 2011, 23(5): 544-553.

[9] LI Z W, HUAI W X, YANG Z H. Interaction between wall jet and offset jet with different velocity and offset ratio [J]. Procedia Engineering, 2012, 28: 49-54.

[10] MONDAL T, DAS M K, GUHA A. Numerical investigation of steady and periodically unsteady flow for various separation distance between a wall and an offset jet [J]. Journal of Fluids and Structures, 2014, 50: 528-546.

[11] MONDAL T, GUHA A, DAS M K. Computational Study of periodically unsteady interaction between a wall jet and offset jet for various velocity ratio [J]. Computers and Fluids, 2015, 123: 146-161.

[12] MONDAL T, GUHA A, DAS M K. Effect of bottom wall proximity on the unsteady flow structures of a combined turbulent wall jet and offset jet flow [J]. European Journal of Mechanics B/Fluids, 2016, 57: 101-114.

[13] CHEN S, DOOLEN G D. Lattice Boltzmann method for fluid flow [J]. Annual Review of Fluid Mechanics, 1998, 30(1): 329-364.

[14] SANI R L, GRESHO P M. Resume and remarks on the open boundary condition minisymposium [J]. International Journal for Numerical Methods in Fluids, 1994, 18(10): 983-1008.

[15] YUAN C C. Control of jet flow mixing and stabilization [D]. San Diego: University of California, 2002.

[16] ZHAO L Q, SUN J H, XU C Y. Flow field analyses of plane jet at low-Reynolds numbers using lattice Boltzmann method [J]. Transactions of Nanjing University of Aeronautics & Astronautics, 2012, 29 (3): 199-206.

[17] ZHAO L Q, SUN J H, XU C Y. Oscillation phenomena in far field region of plane jets at low-Reynolds numbers [J]. Transactions of Nanjing University of Aeronautics & Astronautics, 2013, 30 (1): 17-23.

[18] GUO Z L, ZHENG C G, SHI B C. Discrete lattice effects on the forcing term in the lattice Boltzmann method [J]. Physical Review E, 2002, 65 (4): 046308.

[19] QIAN Y H, D'HUMIERES D, LALLEMAND P. Lattice BGK models for Navier-Stokes equations[J]. Europhysics Letters, 1992, 17(6): 479-484.

[20] SATO H, SAKAO F. An experimental investigation of the instability of a two-dimensional jet at low-Reynolds numbers [J]. Journal of Fluid Mechanics, 1964, 20(2): 337-352.

[21] PEACOCK T, BRADLEY E, HERTZBERG J, et al. Forcing a planar jet flow using MEMS [J]. Experiments in Fluids, 2004, 37(1): 22-28.

[22] JACKSON C P. A finite-element study of the onset of vortex shedding in flow past variously shaped bodies [J]. Journal of Fluid Mechanics, 1987, 182: 23-45.

[23] KUMAR A. Mean flow characteristics of a turbulent dual jet consisting of a plane wall jet and a parallel offset jet [J]. Computers & Fluids, 2015, 114: 48-65.

Dr. **Zhao Liqing** received her B. S., M. S. and Ph. D. degrees in Man-Machine and Environmental Engineering from Nanjing University of Aeronautics and Astronautics in 2004, 2007 and 2013, respectively. She joined in Nanjing University of Information Science & Technology in October 2013, where she is a lecturer of School of Maring Sciences. Her research is focused on computational fluid dynamics and geophysical fluid mechanics.

Prof. **Sun Jianhong** received his B. S. and M. S. degrees in Aerodynamics from Nanjing University of Aeronautics and Astronautics in 1989 and 1996, respectively. He received the Ph. D. degree in Mechanical Engineering from Hong Kong University of Science & Technology in 2001. His research is focused on environmental fluid mechanics and man-machine and environmental engineering.

(Executive Editor: Zhang Tong)